Title

MOBILITY EXPERIMENTS ASSESSING PERFORMANCE OF FRONT-BACK DIFFERENTIAL DRIVE VELOCITY ON SANDY TERRAIN

ISBN

9781942112525

Authors

Cao, C
Creager, C
Lieu, DK
et al.

Publication Date

2021

MOBILITY EXPERIMENTS ASSESSING PERFORMANCE OF FRONT-BACK DIFFERENTIAL DRIVE VELOCITY ON SANDY TERRAIN

Cyndia Cao[a], Colin Creager[b], Dennis K. Lieu[a], and Hannah S. Stuart[a]

[a] *University of California, Berkeley, CA 94709*
[b] *NASA Glenn Research Center, OH 44135*
cyndia_cao@berkeley.edu

Abstract
Sand traps are a hazard for both Martian and lunar rovers. Conventional drive control methods aim to limit wheel slip without considering the effect that both slippage and sinkage have on the forces generated by a rotating wheel. Sandy terrain models, such as granular Resistive Force Theory (RFT), suggest that mobility can be improved by driving the front and back wheels at different angular velocities according to their differing sinkage depths. In this experiment, the effect of the front-back wheel speed ratio on the rover's forward velocity is measured while applying a resistance load to imitate the resistance of climbing a slope. The maximum rover velocities occur at front-back wheel speed ratios at or below 1, when the back wheels drive faster than the front wheels, and the benefit of faster back wheel speeds becomes more pronounced as resistance load increases. In the highest resistance scenario with a drawbar pull to weight ratio of 43% (effective slope angle of 24°), the rover velocity increases by 10% when the back wheels are driven 2.5 times faster than the front wheels. In challenging areas of high slip and sinkage, front-back differential drive control has the potential to enable the rover to achieve more efficient traversal without any modification to existing design and control practices.

Keywords: Planetary Rover, Sandy Terrain, Granular Resistive Force Theory

1. Introduction

Sand traps are a hazard for both Martian and lunar rovers. On Mars, sand or other low-bearing-strength terrain can be hidden under a friable surface that appears solid, and it is difficult to visually estimate the mechanical properties of sand even when visible since its properties are also influenced by sub-surface composition (Chhaniyara et al., 2012). On the moon, water ice is observed in the polar regions, where the surface is covered in craters with steep, loose regolith slopes (Li et al., 2018). Reliable mobility in these types of challenging environments enables critical prospecting missions for in-situ resource utilization.

Wheel slip – the relative velocity between terrain and a rotating wheel – is inherent to wheeled driving in soft granular terrain. Wheel slip is defined mathematically by its angular velocity ω, radius r, and translational velocity v as:

$$\text{slip} = \frac{\omega r - v}{\omega r} = 1 - \frac{v}{\omega r} \quad (1)$$

Conventional drive control methods typically use rover kinematics and velocity control to minimize or eliminate slip on all wheels. Torque control has also been investigated to avoid initiating soil failure (Iagnemma and Dubowsky, 2004), but it is difficult to fully characterize variable terrain enough to perform the calculations required (Gonzalez and Iagnemma, 2018). On a flat homogeneous surface, a typical velocity controller would command all wheels to identical

speeds, which produces equal slip on all wheels. However, in soft terrains, each wheel may sink to a different extent, and the forward tractive force capability of a single wheel depends on both sinkage depth and slip. Force analysis, presented in this paper, shows that the drive torque applied by the wheels consequently increases contact loads and sinkage on the back wheels. This sinkage difference between front and back wheels is exaggerated by low-strength and sloped terrains. Driving the wheels at identical speeds may produce suboptimal tractive force, especially in sloped, sandy environments.

Work by Orton (2019) supports the hypothesis that forward thrust may be improved by varying the commanded speed between the leading and trailing wheels in a 2-wheel system. They measure approximately 18-25% drawbar pull improvement when driving the back wheel twice as fast as the front wheel across many total vehicle slip conditions. This experiment was performed by constraining vehicle and wheel movement and measuring the resulting forces. In the present work, differential drive velocity is investigated with an unconstrained 4-wheeled vehicle with a preset resistance force to generate more realistic driving motions.

In order to evaluate the mobility change produced by driving the front and back wheels at different rates with an unconstrained four-wheeled rover, a fixture is developed to apply a resistance load to the rover and measure the resulting steady state speed as the wheel speed ratios are varied. Force analysis using granular Resistive Force Theory (RFT) to model each wheel is used to predict the velocity trends, and the results are compared. In high sinkage, high slip scenarios, rover velocity can be improved by driving the back wheels faster than the front wheels. Slip is generally regarded as a source of power loss which should be reduced indiscriminately, but an alternative framework to consider is the efficient distribution of slip among driving wheels.

2. Analysis

Granular Resistive Force Theory is a closed-form empirical model useful for rapidly estimating drag and lift forces acting on a body moving through dry granular media such as sand (Li et al., 2013). This force model is based on penetrometry studies of several different media consisting of homogeneous, mostly spherical and smooth particles. Its performance is comparable to the Bekker-Wong model at predicting the mobility metrics of single, slip-controlled wheels of various shape in Martian sand simulants (Agarwal et al., 2019). The model can also be applied to arbitrary 3D wheel shapes and trajectories (Treers et al., 2021). Algebraic analysis based on RFT and validation by DEM simulations show that non-dimensionalization of a wheel's mass, velocity, and power can enable close prediction of vehicle performance in a single media but across differing gravity levels (Slonaker et al., 2017). Since the media is defined only by a single scaling coefficient, its value can be modified to understand the sensitivity of a robot to the "softness" or "stiffness" of the terrain, which can be affected by gravity. Its calculation speed, compared with computational approaches like Discrete Element Method (DEM), and simplicity, not requiring as many soil- and wheel-specific parameters as the Bekker-Wong model, enable quick insights into the mechanism and control design spaces for robots that must locomote through sand.

Given a wheel's geometry and motion, i.e. sinkage depth, driven angular velocity, and translational velocity, granular RFT predicts the forces along the wheel-sand contact surface, which can be integrated to calculate the total forces and torques on the wheel, accounting for both thrust and resistance due to wheel-terrain interaction. These forces are a function of wheel slip and sinkage as shown by the contour plots of Fig. 1. These contours are generated for a cylindrical wheel with radius 1m and width 1m and a media with RFT scaling coefficient of 1 (previously measured sands have a coefficient of 2-5) to demonstrate the non-linear trends. The contour values can be scaled according to the wheel dimensions and media of interest. Figure 1a illustrates the drawbar pull, or net forward tractive force generated by the wheel after deducting resistive forces, and notably shows that as wheel depth increases, more slip is necessary to generate forward traction rather than backward resistance (grey shaded region). The negative contour lines in the shaded region are closer than in the positive, unshaded region, and they demonstrate that increasing sinkage quickly impedes vehicle motion. Figure 1b suggests that the required drive torque asymptotes above 20% slip to a value that is dependent solely on wheel sinkage. Figure 1c combines 1a and 1b to produce an efficiency metric, the level of drawbar pull output generated by a given torque input. Like Fig. 1a, this indicates that wheels at deeper sinkage depths need to slip more to maintain efficient mobility. Finally, Fig. 1d shows the vertical load that a wheel can support given a slip and sinkage; for a fixed load, increasing slip will gradually increase sinkage.

Each wheel in a rover will act at a different slip and sinkage coordinate on these contour plots, which informs how each wheel contributes to the vehicle's overall motion. The free body diagram shown in Fig. 2 is used to estimate the steady state driving configuration. A horizontal resistance load is applied to the vehicle to mimic the effect of vehicle weight impeding progress up a sandy slope. Each wheel is velocity-controlled, and the average commanded velocity is

held constant while the front-back speed ratio $\omega_{\text{front}}/\omega_{\text{back}}$ varies. Vehicle velocity and wheel sinkage depths are estimated by solving for the front and back wheel slip and sinkage that results in steady state (equilibrium) behavior, i.e. constraining total forces and moments to be balanced. Due to the moment balance constraint, when greater drive torques are applied by the wheels, the rear wheels must support a larger share of the weight of the vehicle. If all wheels are controlled solely to minimize or match slip, the wheels with greater sinkage depth, which are generally the rear wheels, will produce drawbar pull less efficiently. This suggests that in challenging scenarios which result in high wheel sinkage, and specifically high differences between front and back wheel sinkage, vehicle mobility may be improved by driving or slipping the wheels at different levels.

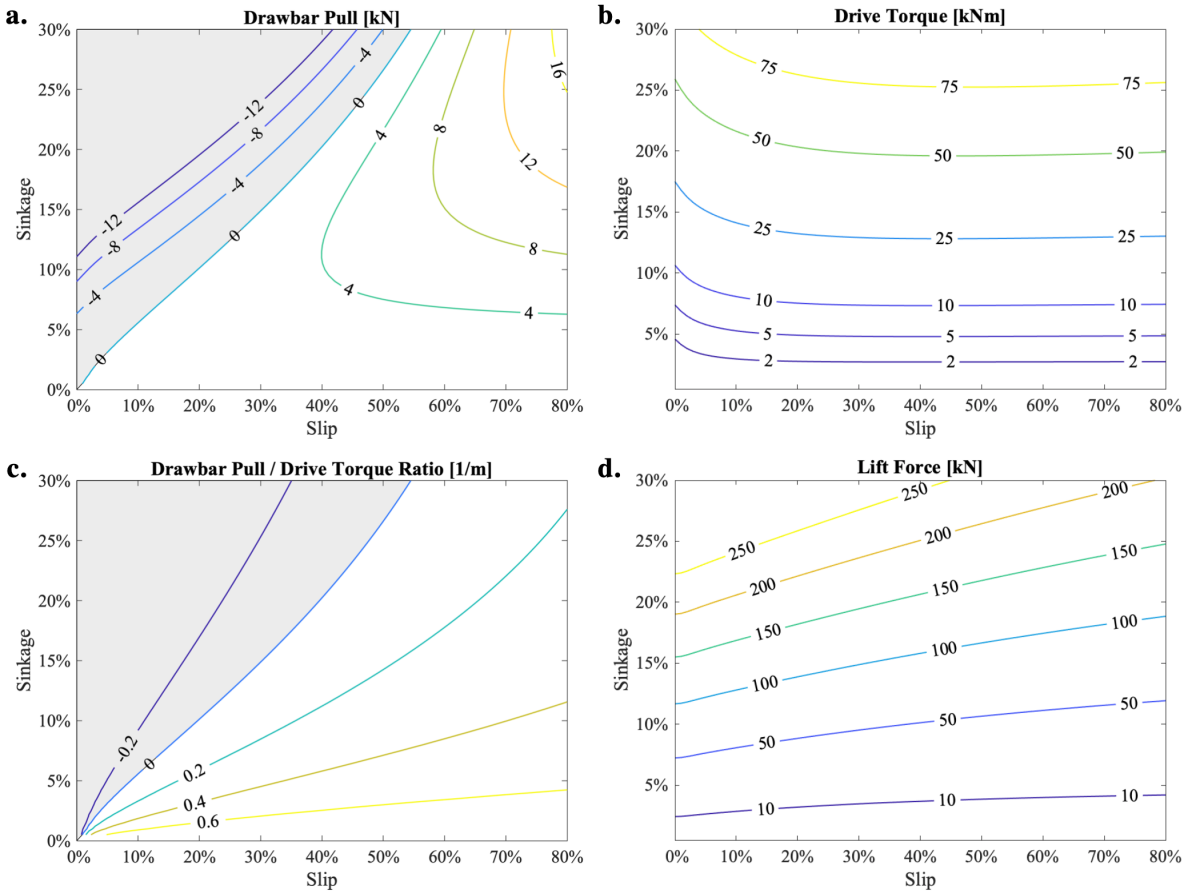

Fig. 1. *Contour plots that illustrate the steady state forces and torques on a wheel given a specified slip and sinkage depth, as predicted by granular RFT. These contour levels assume a wheel radius of 1m, width of 1m, and RFT coefficient of 1, but the values can be scaled according to arbitrary geometry and media. Sinkage is represented relative to the full wheel diameter.*

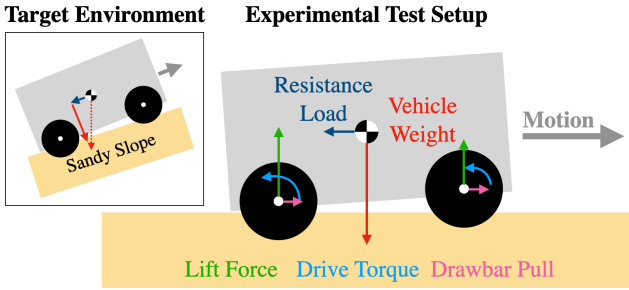

Fig. 2. *A free body diagram depicting the vehicle loads and the forces generated at the wheels by driving in sand. A resistance load is applied to the vehicle driving on flat ground to imitate the effect of vehicle weight on a sandy slope.*

Figure 3 shows the trends predicted by RFT given the present experimental setup. The maximum rover velocity occurs when the back wheels are driven faster than the front wheels (speed ratio < 1), and the peak velocities marked in Fig. 3a moves left as the resistance load increases. Fig. 3b confirms that the force-moment balance predicts greater sinkage on the back wheel, which suggests that it will operate with a different locomotive efficacy as the front wheel. Finally, the results are non-dimensionalized in Fig. 3c so that the results can be generalized and compared in future work with different vehicle configurations. The metric of travel reduction (TR), defined below in Eq. 2, is used since a single wheel slip value can no longer capture the dynamics of the vehicle. As a reference "ideal" velocity v_{baseline}, TR uses the velocity of a vehicle driving both wheels at the average wheel angular rate $(\omega_{\text{front}} + \omega_{\text{back}})/2$ with no slip, and v_{actual} is the overall velocity of the vehicle.

$$\text{TR} = \frac{v_{\text{baseline}} - v_{\text{actual}}}{v_{\text{baseline}}} = 1 - \frac{v_{\text{actual}}}{\omega_{\text{avg}} r} \tag{2}$$

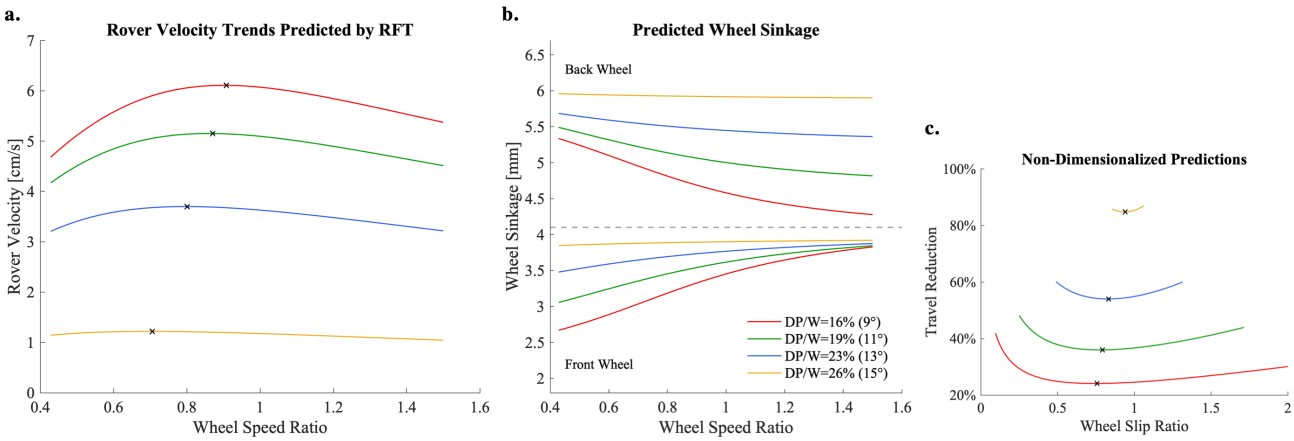

Fig. 3. *Rover velocity and wheel sinkage trends as predicted by RFT. Each line corresponds to a different drawbar pull (resistance load) per vehicle weight ratio, and an inverse tangent relation is used to estimate the analogous slope angle shown in parentheses.*

3. Experimental Setup

Differential drive velocity is investigated at various analogous slope angles by applying a constant resistance load to the vehicle and commanding the front and back wheels to drive at a range of different velocities. Mobility is evaluated by measuring vehicle forward velocity, drive motor current, and wheel sinkage.

The test track is 1.5 m long, 66 cm wide, and 20 cm deep and is filled with Sakrete All Natural Play Sand. Vertical plate penetration tests measure the RFT coefficient of this sand to be approximately 4. The test vehicle is a rigid platform with four individually driven wheels (ServoCity Prowler), which are each velocity-controlled by RoboClaw motor controllers. Each wheel is 3D printed with a diameter of 17.5 cm and width of 15.5 cm, and they are circumscribed with 20 grousers of 5 mm height and width. The rover has a wheelbase of 23 cm and a total track width of 37.5 cm.

A constant resistance force is applied to the rover via a tensioned cable, as shown in Fig. 4. The cable is attached to the rover at a height approximately in line with the center of the chassis to minimize front-back weight transfer caused by the application of force. The vertical position of the lowest pulley is adjusted with each resistance force value such that the cable is level during baseline steady state driving, when both wheels drive at the same speed. The resistance force determines the magnitude of drawbar pull that the vehicle must generate to drive forward. The ratio of the drawbar pull to vehicle mass can help predict the ability of a rover to climb slopes, where the resistance force represents the downhill force due to the weight of the rover, as depicted in the inset of Fig. 2.

Two distance sensors on the vehicle, aligned with the front and back wheels, estimate sinkage by measuring the distance between the chassis and the undisturbed sand surface. The RoboClaw motor controllers measure the current pulled by each drive motor. Finally, a distance sensor attached to the resistance weight carriage measures the speed of the rover, assuming an inextensible tension cable connecting the load to the vehicle.

Resistance force and wheel speed ratio stay constant throughout each individual trial, during which the rover drives across the full length of the sandbox while the steady state parameters (rover velocity, wheel sinkage, and motor power) are recorded. Between trials, the wheel speed ratio $\omega_{\text{front}}/\omega_{\text{back}}$ varies, while the total wheel speed $\omega_{\text{front}} + \omega_{\text{back}}$ remains constant. Each speed ratio is tested five times per resistance force level, and four force levels are used to observe the effect of varying wheel speed ratio across a spectrum of terrain difficulty.

The sand is reset between each trial to promote consistency, as illustrated in Fig. 5. The process consists of stirring the surface with a rake and shovel, penetrating roughly 10 cm and resulting in a pile on one end of the sandbox. Then a wooden beam is pulled along the sandbox length to level the surface, constrained by rails along the length of the sandbox to avoid re-compaction. Before starting trials at a new resistance level, and if the load cell reports inconsistent forces between trials, the pulley shafts are wiped down and re-lubricated; otherwise sand and grit generate undesirable friction as they build up on the weighted pulley system.

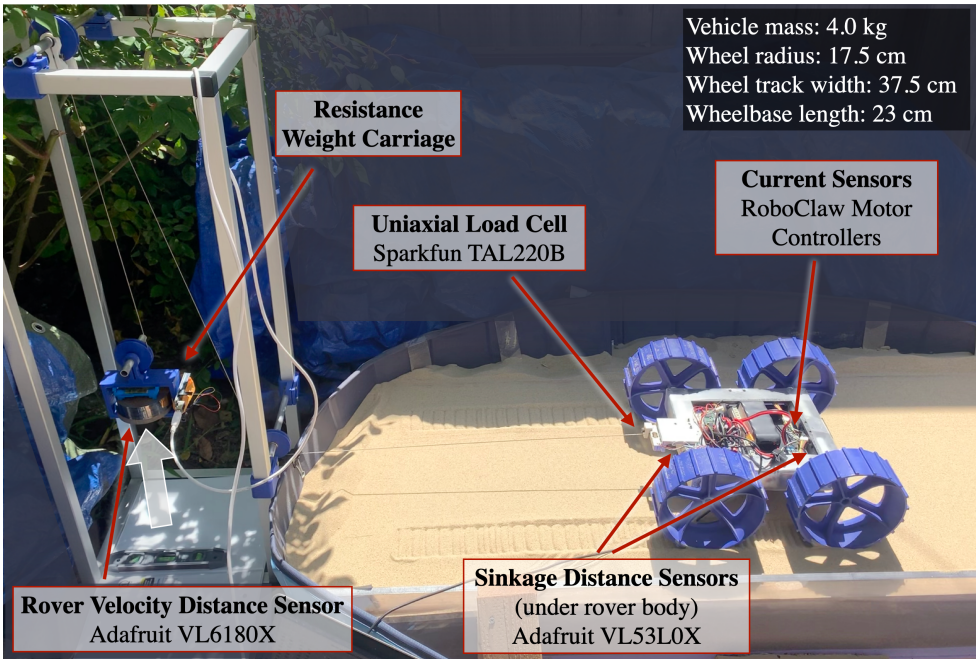

Fig. 4. *Experimental setup. A fixed resistance load is applied to the vehicle via a tensioned cable. The front-back wheel speed ratio varies between trials, while the vehicle velocity, wheel sinkage, and motor currents are measured.*

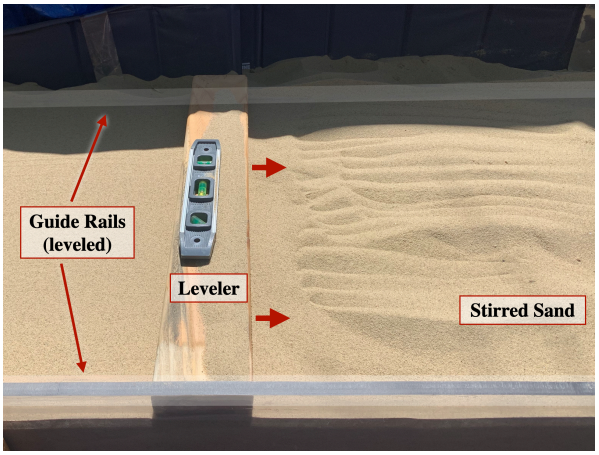

Fig. 5. *Sand reset process. First the entire track is stirred using hand shovels and rakes. Then a wooden beam slides along two guide rails to re-level the surface without significant re-compaction of the sand.*

4. Results and Discussion

Across all drawbar pull conditions, maximum rover velocity occurs at front-back wheel speed ratios below or at 1, or when the back wheels drive faster than the front wheels, shown in Fig. 6a. The benefit of front-back differential drive becomes more pronounced as resistance load increases, as emphasized in Fig. 6b where the rover velocity is normalized at the wheel speed ratio of 1. For instance, in the highest resistance scenario of DP/W = 43%, the rover velocity increases by 10% when the back wheels rotate 2.5 times faster than the front wheels (wheel speed ratio of 0.4) as opposed to when they drive at equal speeds. Even at the lower resistance levels, there is generally a plateau region where driving the back wheel slightly faster than the front wheel is comparable to conventional equal speed driving. A non-dimensionalized form of the data is shown in Fig. 7, using axes of travel reduction and wheel slip ratio.

The shape of the velocity-speed ratio curves measured in the experiment match the trends generated in the RFT predictions using the same vehicle parameters and measured terrain coefficient. The grousers are not included in the model, so it predicts that the rover will fail to drive at lower loads (note the difference in DP/W levels in the legend). Subsequently the wheel sinkage depths are also less than observed. It is also possible that the resistance cable caused some level of weight transfer between the wheels, despite efforts to minimize this effect. The load conditions in Fig. 3

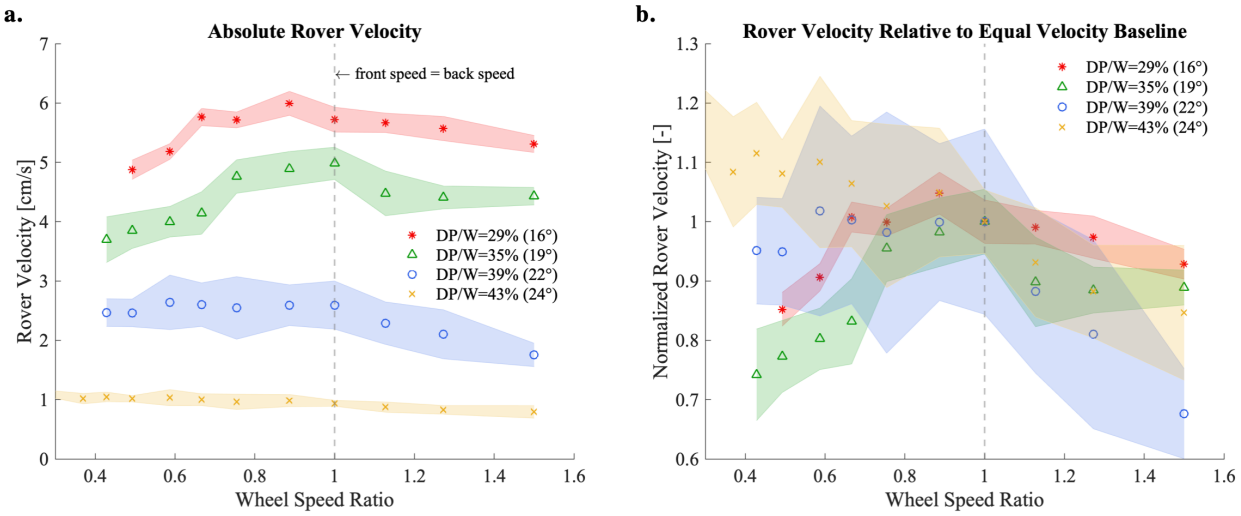

Fig. 6. *Measured rover velocity as a function of front-back wheel speed ratio. When the speed ratio is less than 1, the back wheels drive faster than the front wheels. In scenarios with high drawbar pull coefficient DP/W, the maximum rover velocity occurs at lower wheel speed ratios.*

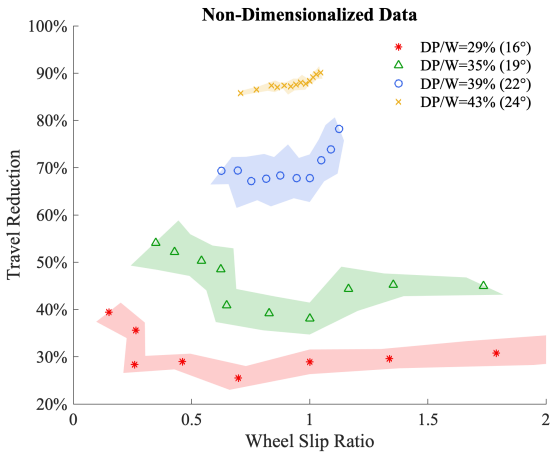

Fig. 7. *Rover velocity data non-dimensionalized into travel reduction and wheel slip ratio.*

are chosen such that the highest and lowest loads produce peak velocities that are comparable to the data, and the intermediate loads are equally spaced between them. RFT predicts that the vehicle will see 90% travel reduction when the resistance force reaches 26% of the vehicle's weight, but this happens experimentally at a load ratio of 43%. Notably, the trends predicted by the model are observed in the experimental data, even though there is variation in the absolute values.

This variation is likely also caused by a combination of real-world granular interactions which are not captured by RFT, such as mounding, compaction, and particle size distribution. Single wheel tests with controlled slip produce forces very close to those predicted by RFT, but the surface is always pristine. The sand mounds created behind driving wheels change the condition of the sand that must be traversed by subsequent wheels, and this is unaccounted for. Although the front wheels sink less deep and Fig. 1c suggests that they therefore produce drawbar pull more efficiently, high front wheel slip increases the height of the sand pile left behind the front wheels. These piles pose a challenge for the back wheels, which already sink deeper due to the force distribution of the rover. Reducing front wheel slip reduces the size of the obstacle that the back wheels must climb, so the consequence of surface mounding may amplify the benefit of low wheel speed ratios. If better absolute predictive performance is necessary, multi-pass effects should be included to capture the disturbances created by wheel ruts and mounds.

Additionally, RFT assumes that the forces on a surface element of the body increase linearly with intrusion depth, and the scaling coefficient is measured at a depth of interest. With the experimental media, a natural sand, the coefficient increases moderately with depth, which may explain why the vehicle generates more drawbar pull than predicted as its wheels sink further into the sand. Furthermore, the front wheels may compact the sand such that its RFT scaling coefficient increases and the back wheels can more effectively generate drawbar pull. While the assumptions of granular RFT limit its absolute accuracy, RFT effectively predicts the observed trends, and its force model provides a feasible explanation for the observed benefits of front-back differential velocity control.

As shown in Fig. 7, wheel sinkage and drive motor current increase with drawbar pull. The motors' baseline current draw, which is measured by driving the rover in the air, is subtracted from the raw measurements to produce Fig. 7a. The back wheels pull significantly more current than the front wheels, which indicates that they are more heavily loaded. As the back wheels drive faster or slip more, the current draw from the back motors increases and from the front motors decreases. Consequently, when generating high drawbar pull, the maximum rover velocity is achieved by increasing load on the back drive motors, rather than distributing load more evenly. This result is in line with previous torque control work, which asserts that more torque should be applied by wheels which experience higher normal load since the terrain underneath can support more tractive force (Iagnemma and Dubowsky, 2004). As the back wheel slip increases, the back wheels experience more sinkage and the front wheels rise; the RFT model correspondingly predicts that high slip reduces the lift force generated by a spinning wheel. Note that the wheel sinkage sensors measure the

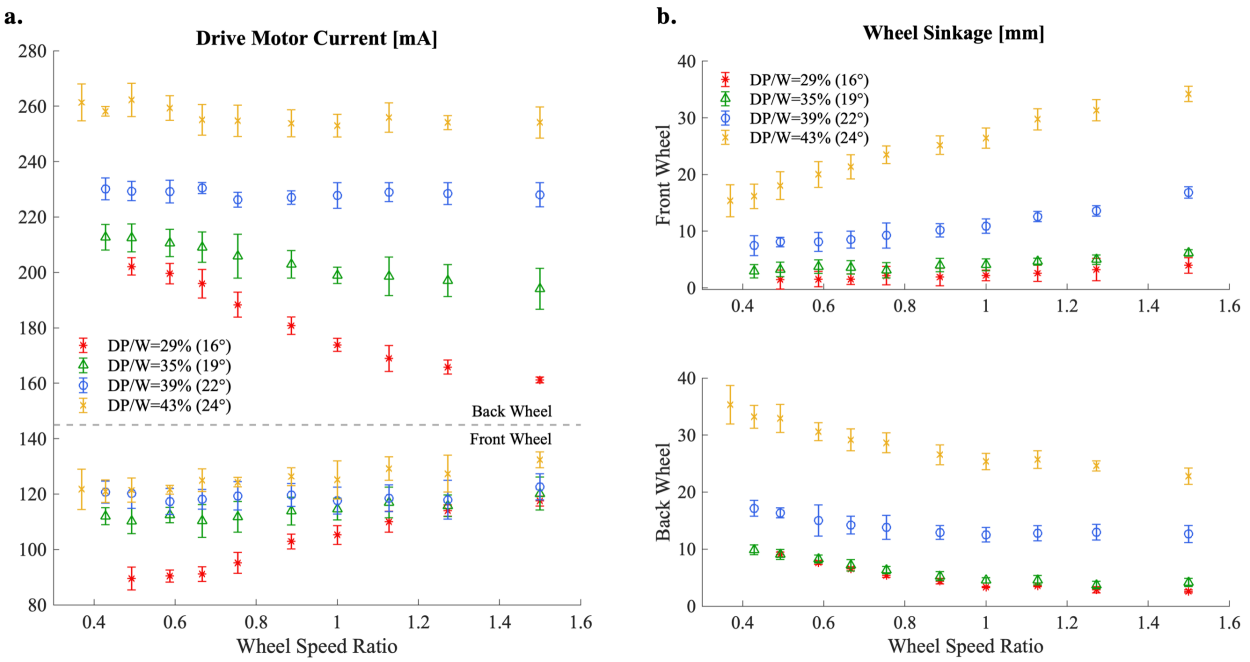

Fig. 8. *Measured motor currents and wheel sinkage.*

displacement of the front and back of the chassis relative to a flat rigid surface, but they do not indicate the sinkage of the back wheel relative to the sand pile that is created behind the front wheel.

Using the motor current and rover velocity data from Fig. 7 and Fig. 8, a power efficiency comparison is shown in Fig. 9. The battery is assumed to stay at 12V, and the power is the sum of all power consumed by the drive motors. Efficiency is calculated as the power required to achieve a unit velocity, which can also be interpreted as the energy required to traverse a certain distance. The total power required by these motors is relatively insensitive to the wheel speed ratio, which results in improved energy efficiency when the vehicle achieves greater velocity. This preliminary analysis suggests that the goal of increasing rover velocity is symbiotic with improving power efficiency, which is a critical mobility metric of planetary exploration rovers.

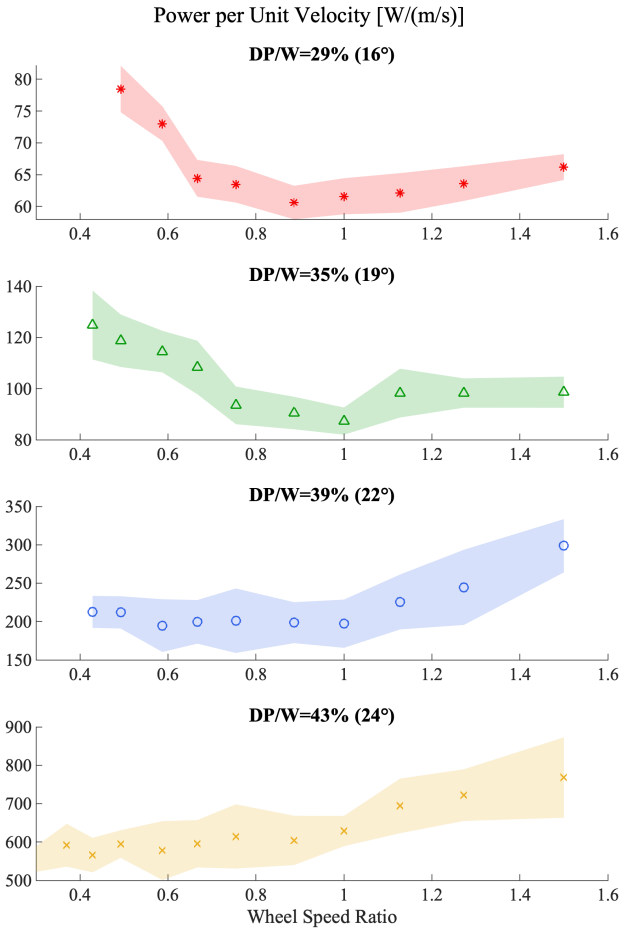

Fig. 9. *Power consumed per 1 m/s velocity generated by the vehicle in each resistance scenario. Power consumption did not change significantly across wheel speed ratios, which results in improved efficiency when the rover is able to drive faster.*

5. Conclusion

There is potential to improve the travel efficiency of 4-wheeled planetary rovers by driving the back wheels faster than the front wheels, particularly on soft sands or where high drawbar pull is required. Granular RFT suggests that increased sinkage in rear wheels causes them to experience different forces than the front wheels, and this implies that velocity matching among all wheels is not always optimal. Velocity improvements via front-back differential drive velocity control are most notable in high sinkage and slip scenarios. On flat, low-slip surfaces with little sinkage, the existing standard of driving the wheels at the same speed remains preferred as it prevents fighting between wheels and distributes the tractive load between wheels. However, in challenging areas where front and back wheels may sink to varying depths, differential drive control can assist the rover achieve more efficient traversal, both with respect to travel

time and power efficiency. Prior work with constrained vehicle motion suggests up to 25% improvement in drawbar pull capacity with a wheel speed ratio of 0.5, while the present unconstrained vehicle only achieves a 10% increase in velocity. The difference in these outcomes motivates further research to understand how vehicle or terrain parameters influence the efficacy of differential velocity driving.

Finally, this type of control can be implemented on a variety of rover platforms without any hardware modification. It can be executed on already existing rovers and without much change to conventional design and control practices, so it is valuable to explore further in more realistic scenarios. Future work should refine this finding by testing a rover of weight class and size that has a representative ground pressure distribution and perform the experiment in loose sand on a slope-controlled bed, where the sand may exhibit different mobilization behavior. Steepest traversable slope angle and power efficiency can then be analyzed more rigorously in order to inform future planetary rover control.

Acknowledgements

This work was supported by a NASA Space & Technology Fellowship, grant number 80NSSC19K1167 Mobility Evaluation of a Planetary Rover with Gyroscopic Force Redistribution Control.

References

Agarwal, S., Senatore, C., Zhang, T., Kingsbury, M., Iagnemma, K., Goldman, D.I., Kamrin, K., 2019. Modeling of the interaction of rigid wheels with dry granular media. J. Terramechanics 85, 1–14.

Chhaniyara, S., Brunskill, C., Yeomans, B., Matthews, M.C., Saaj, C., Ransom, S., Richter, L., 2012. Terrain trafficability analysis and soil mechanical property identification for planetary rovers: A survey. Journal of Terramechanics 49, 115–128. https://doi.org/10.1016/j.jterra.2012.01.001

Gonzalez, R., Iagnemma, K., 2018. Slippage estimation and compensation for planetary exploration rovers. State of the art and future challenges. J. Field Robotics 35, 564–577. https://doi.org/10.1002/rob.21761

Iagnemma, K., Dubowsky, S., 2004. Rough Terrain Control, in: Mobile Robots in Rough Terrain: Estimation, Motion Planning, and Control with Application to Planetary Rovers, Springer Tracts in Advanced Robotics. pp. 81–96.

Li, C., Zhang, T., Goldman, D.I., 2013. A Terradynamics of Legged Locomotion on Granular Media. Science 339, 1408–1412. https://doi.org/10.1126/science.1229163

Li, S., Lucey, P.G., Milliken, R.E., Hayne, P.O., Fisher, E., Williams, J.-P., Hurley, D.M., Elphic, R.C., 2018. Direct evidence of surface exposed water ice in the lunar polar regions. Proc Natl Acad Sci USA 115, 8907–8912. https://doi.org/10.1073/pnas.1802345115

Orton, K., 2019. Analysis of Inching for Planetary Rover Exploration (Master's thesis). Carnegie Mellon University, Pittsburgh, PA.

Slonaker, J., Motley, D.C., Zhang, Q., Townsend, S., Senatore, C., Iagnemma, K., Kamrin, K., 2017. General scaling relations for locomotion in granular media. Phys. Rev. E 95, 052901. https://doi.org/10.1103/PhysRevE.95.052901

Treers, L.K., Cao, C., Stuart, H.S., 2021. Granular Resistive Force Theory Implementation for Three-Dimensional Trajectories. IEEE Robot. Autom. Lett. 6, 1887–1894. https://doi.org/10.1109/LRA.2021.3057052